

## Measurement of the Inclusive Neutron Production by Relativistic Neon Ions on Uranium

Walter Schimmerling, John W. Kast, and Douglas Ortendahl<sup>(a)</sup>  
*Lawrence Berkeley Laboratory, Berkeley, California 94720*

and

Richard Madey, Robert A. Cecil, Bryon D. Anderson, and Alan R. Baldwin  
*Department of Physics, Kent State University, Kent, Ohio 44242*  
 (Received 5 November 1979)

Inclusive double-differential cross sections for neutron production were measured at 337 MeV/nucleon in the reaction  $\text{Ne} + \text{U} \rightarrow n + X$ . Neutrons were detected with energies between  $\sim 12$  and  $\sim 600$  MeV at laboratory angles of  $30^\circ$ ,  $45^\circ$ ,  $60^\circ$ , and  $90^\circ$ . The neutron spectra above  $\sim 30$  MeV are comparable with the predictions of a "firestreak" calculation. The neutron spectra differ from proton spectra reported for U and Pb.

We measured the double-differential cross sections for neutron production by 337-MeV/nucleon neon ions interacting in uranium targets. The experiment was carried out at the Bevalac accelerator of the Lawrence Berkeley Laboratory (LBL).

Figure 1 is a scale drawing of the experimental cave. The beam traversed a scintillation-counter telescope consisting of a  $20 \times 20\text{-cm}^2$  detector  $S_0$  (not shown in Fig. 1), positioned  $\sim 10$  m

upstream of the target  $T$ , and a  $7.6 \times 7.6\text{-cm}^2$  scintillator  $S_1$  located next to the target. After traversing the target, the beam continued to a 30.5-cm-diam, 1.2-m-deep beam dump. The depleted  $^{238}\text{U}$  targets had an area of  $10 \times 10\text{ cm}^2$  and were positioned at  $45^\circ$  to the beam axis. One of the targets used was  $5.60\text{ g/cm}^2$  thick, while the other one was  $1.86\text{ g/cm}^2$  thick.

Neutrons were detected by four 101.6-cm-wide, 10.2-cm-thick scintillation counters made of NE-102 plastic and positioned at  $30^\circ$ ,  $45^\circ$ ,  $60^\circ$ , and  $90^\circ$ , with flight paths of 5.1, 5.6, 6.0, and 4.2 m, respectively. The  $30^\circ$  and  $45^\circ$  detectors were 12.7 cm high. The  $60^\circ$  and  $90^\circ$  counters were 25.4 cm high. Charged particles incident on the detectors were vetoed with 6-mm-thick plastic scintillators in front of each counter.

The background originating in the material around and upstream of the target was determined by taking data with a dummy target holder in place. Target-correlated background was determined from measurements with and without the shadow bars shown in Fig. 1. The shadow bars consisted of 91.5-cm-thick and 60-cm-wide assemblies of lead bricks, located halfway between the target and a detector. A 12.5-cm-high shadow bar was used at  $30^\circ$  and  $45^\circ$ ; at  $60^\circ$  and  $90^\circ$ , the shadow bar was 20 cm high. The shadow bars attenuated neutrons by a factor  $> 100$  at all energies.

The kinetic energy of each detected neutron was obtained from the measured time of flight (TOF) between  $S_0$  and any of the detectors. The neutron detection time was determined by mean timing of signals from both ends of each counter.<sup>1</sup> The light output of each detector was measured separately as the sum of signal amplitudes from the two photomultipliers. The neutron-detector efficiencies were calculated with a Monte Carlo code estimated to be accurate to  $\sim 5\%$  (excluding

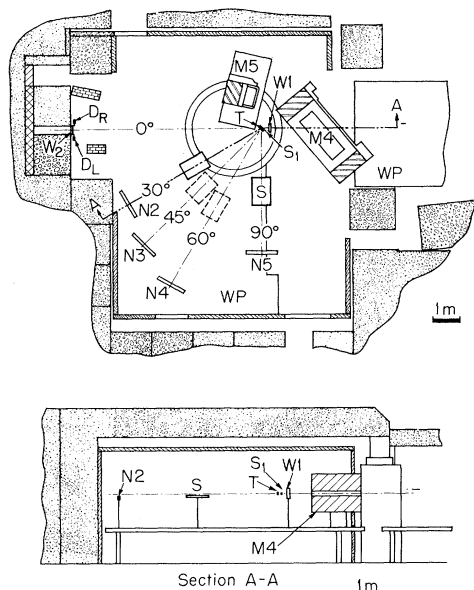


FIG. 1. Scale drawing of the experimental arrangements.  $S_1$ , scintillation counter;  $T$ , target;  $N_2 - N_5$ , neutron detectors;  $S$ , shadow bar in position;  $D_R$  and  $D_L$ , scintillation counters for monitoring beam position;  $WP$ , wooden platform. The beam positioning wire chambers  $W1$  and  $W2$  were removed for data taking. Magnets  $M4$  and  $M5$  were not used but are shown as possible sources of background.

threshold uncertainties), on the basis of comparisons with available experimental data.<sup>2</sup> An unambiguous determination of TOF required that one, and only one, beam particle be incident on the target during the 200-nsec sampling time; therefore, pileup circuitry rejected beam pulses in  $S_0$  which were accompanied by a second pulse within  $\pm 200$  nsec. Use of high-current, high-counting-rate photomultiplier bases<sup>3</sup> allowed a beam counting rate of  $\sim 5 \times 10^5$  per pulse with a rejection ratio of 30–40%.

Figure 2 is a plot of the double-differential cross sections  $d^2\sigma/dTd\Omega$  as a function of neutron energy. The solid curves are the results of a firestreak calculation (neglecting Coulomb effects) by Westfall.<sup>4</sup> Errors include statistics and small effects of uncertainties in the time calibration. The error bars are generally smaller than the size of the symbols. The principal sources of systematic errors are detector efficiencies, target thickness, and beam normalization. The uncertainties in the threshold increase the uncertainties in the efficiencies from  $\sim 5\%$  above 18 MeV to  $\sim 10\%$  at 12 MeV. The overall systematic error is estimated to be  $\sim 10\%$ .

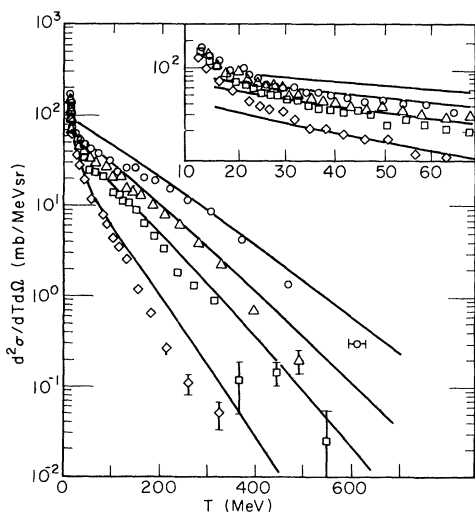


FIG. 2. Measured double-differential cross sections for  $\text{Ne} + \text{U} \rightarrow n + X$  at a mean incident energy of 337 MeV/nucleon, as a function of neutron energy (circles,  $30^\circ$ ; triangles,  $45^\circ$ ; squares,  $60^\circ$ ; lozenges,  $90^\circ$ ), and results of a firestreak calculation (solid curves). Inset: Expanded view of the low-energy portion of the spectra. Errors include statistics and small effects of uncertainties in the time calibration on the width of the energy bin, and on the mean energy of each point. Error bars are generally smaller than the symbol sizes.

The cross sections for different angles approach similar values below 20 MeV, as expected for isotropic neutron evaporation from the target. The neutron spectra at higher energies can be considered as the combination of a broad peak and an approximately exponential spectrum predicted by the firestreak model. Such an interpretation is suggested by the prominent shoulder in the  $30^\circ$  spectrum. The maxima obtained by decomposing the spectra in this manner are at  $\sim 250$ ,  $\sim 200$ , and  $\sim 130$  MeV at  $30^\circ$ ,  $45^\circ$ , and  $60^\circ$ , respectively. The large angles and the energies at which shoulders are seen exclude the projectile as a source. It seems more likely that these shoulders are due to a nucleon-nucleon knockout component. The residual portions of the spectra are then found to agree with the firestreak model within a factor of  $\sim 2$ .

The cross sections integrated between 12 and 600 MeV at the four laboratory angles are 9.2, 6.3, 4.4, and 2.2 b/sr. The total angle-integrated cross section in the forward hemisphere is  $\sim 37$  b. Based on a reaction cross section of 4.0 b,<sup>5</sup> the average neutron multiplicity in the forward hemisphere is  $\sim 9$ . This is comparable to reported proton multiplicities.<sup>6</sup>

Figures 3(a)–(d) are plots of the ratio of the measured neutron production cross section to that for the production of protons in similar reactions as a function of energy. The closed circles refer to proton data<sup>6</sup> from 393-MeV/nucleon  $\text{Ne} + \text{U}$ , and the open circles refer to proton data<sup>7</sup> from 385-MeV/nucleon  $\text{Ne} + \text{Pb}$ . The slightly higher ratios obtained for the latter are due to the smaller cross section in Pb. The solid and dashed curves are the  $n/p$  cross-section ratios expected from firestreak calculations (without Coulomb effects)<sup>4</sup> for the appropriate combinations of target and beam energy. Different numbers of neutrons and protons contribute to the projectile-target interaction at different impact parameters. The cross-section ratios given by the firestreak calculations provide a scaling factor for comparison with the experimental data.

The firestreak calculations predict a moderate decrease in the  $n/p$  ratio, varying between  $\sim 1.7$  at 20 MeV and  $\sim 0.9$  at 600 MeV. The data differ significantly from this expectation, especially at low energies, where the measured ratio is  $\sim 2$  times the predicted value. The measured  $n/p$  ratios decrease with energy much more rapidly than predicted.

Since fragments with  $A > 5$  are not considered by the present firestreak calculations, a possible

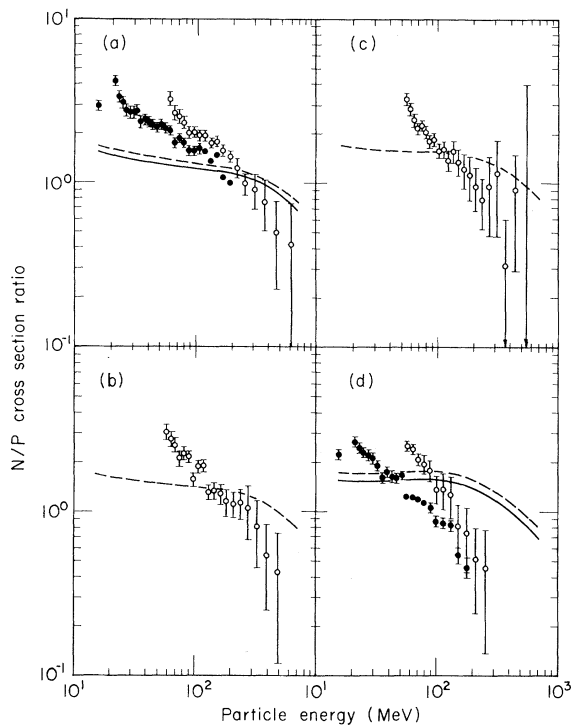


FIG. 3. Neutron to proton cross-section ratios as a function of neutron energy at (a)  $30^\circ$ , (b)  $45^\circ$ , (c)  $60^\circ$ , and (d)  $90^\circ$ . Two sets of ratios are plotted: (I)  $(\text{Ne} + \text{U} \rightarrow n + X \text{ at } 337 \text{ MeV/nucleon}) / (\text{Ne} + \text{U} \rightarrow p + X \text{ at } 393 \text{ MeV/nucleon})$ , see Ref. 6; and (II)  $(\text{Ne} + \text{U} \rightarrow n + X \text{ at } 337 \text{ MeV/nucleon}) / (\text{Ne} + \text{Pb} \rightarrow p + X \text{ at } 385 \text{ MeV/nucleon})$ , see Ref. 7. Full circles: experimental results for I. Open circles: experimental results for II. Solid curve: firestreak calculation for I. Broken curve: firestreak calculation for II.

mechanism for producing an observed neutron excess at low energies is neutron evaporation from excited, neutron-rich fragments. The existence of such fragments would be expected in the absence of equilibrium, when the projectile energy has not been distributed uniformly among the projectile plus target nucleons.

Preliminary results of some recent calculations<sup>8,9</sup> indicate that Coulomb effects suppress

the proton yield at low energies and shift the high-energy part of the proton spectrum toward higher energies. The Coulomb effects seem to be sufficiently large to explain most of the observed results, but a final conclusion will have to await the results of ongoing theoretical work.

We are grateful to the Gesellschaft für Schwerionenforschung–Marburg–LBL collaboration and S. Nagamiya for the use of their data prior to publication, to G. Westfall for the firestreak calculations, and to Y. Karant, M. Gyulassy, H. Gutbrod, and A. Poskanzer for useful conversations and encouragement. The pileup rejection electronics were designed and built at LBL by G. Gabor. We are indebted to him and to M. Strathman for assistance with the electronics. The high-rate photomultiplier bases were constructed by M. Maier.

This work was supported in part by the Office of Health and Environmental Research of the U. S. Department of Energy, by the National Aeronautics and Space Administration, by the U. S. National Science Foundation, and by the U. S. Department of Energy.

<sup>(a)</sup>Present address: Department of Radiology, University of California, San Francisco, Cal. 94143.

<sup>1</sup>A. R. Baldwin and R. Madey, to be published.

<sup>2</sup>R. A. Cecil, B. D. Anderson, and R. Madey, *Nucl. Instr. Methods* **161**, 439 (1979).

<sup>3</sup>C. R. Kerns, *IEEE Trans. Nucl. Sci.* **24**, 353 (1977).

<sup>4</sup>G. Westfall, private communication; J. Gosset, J. I. Kapusta, and G. D. Westfall, *Phys. Rev. C* **18**, 844 (1978). The calculation has taken into account the variation in beam energy along the target.

<sup>5</sup>P. J. Karol, *Phys. Rev. C* **11**, 1203 (1975).

<sup>6</sup>A. Sandoval, H. H. Gutbrod, W. G. Meyer, A. M. Poskanzer, R. Stock, J. Gosset, J. C. Jourdain, C. H. King, G. King, C. H. Lukner, Nguyen Van Sen, G. D. Westfall, and K. L. Wolf, to be published.

<sup>7</sup>M.-C. Lemaire, S. Nagamiya, O. Chamberlain, G. Shapiro, S. Schnetzer, H. Steiner, and I. Tanihata, private communication.

<sup>8</sup>Y. Karant, private communication.

<sup>9</sup>M. Gyulassy, private communication.